THE ARCHIVE OF MECHANICAL ENGINEERING

Vol. LII 2005 Number 4

Key words: *press, crack, compression, initiation, propagation*

GIORGIO OLMI[*)], *ALESSANDRO FREDDI*[**)]

CRACK INITIATION AND PROPAGATION IN A PRESS COLUMN UNDER COMPRESSIVE LOAD

One of the worst accidents that can take place in industrial presses is related to the risk of generating cracks in the columns. In order to avoid press columns from being subjected to tensile stress in the loading phase, the columns are sometimes assembled pre-compressed, so that nominal stress maintains negative values throughout the work cycle.

Previous researches have considered cracks propagating under cyclic compressive loads in notched specimens. In these cases, the fatigue cracks are initiated at the notch root due to residual tensile stresses and grew at a progressively decreasing speed before arresting. The subject of the present paper is to give a paradigmatic example of crack initiation and propagation also in a general compressive field.

SYMBOLS

σ_y = yield strength
E = Young's modulus
K = static strain hardening coefficient
n = static hardening exponent
K' = cyclic strain hardening coefficient
n' = cyclic hardening exponent
σ'_f = fatigue strength coefficient
ε'_f = fatigue ductility coefficient
b = fatigue strength exponent
c = fatigue ductility exponent

*) *D.I.E.M. – Department of Mechanical Engineering – University of Bologna, Viale del Risorgimento, 2, Bologna, Italy; giorgio.olmi@mail.ing.unibo.it*

**) *D.I.E.M. Department of Mechanical Engineering University of Bologna, Viale del Risorgimento, 2, Bologna, Italy; alessandro.freddi@mail.ing.unibo.it*

1. Introduction

Huge industrial presses are composed of a closed frame with two columns and two transverse elements. Compressive load is generated by an oleo-dynamic power pack, which generates the displacement of a piston, whose cylinder is sustained by one of the transverse elements. During the work cycle, when the compressive load is transmitted, the two columns are subjected to relevant tensile stresses, Fig. 1.

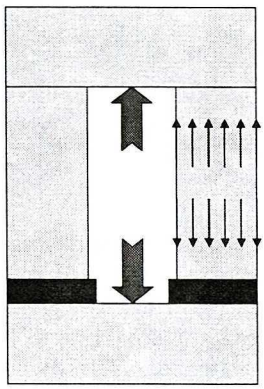

Fig. 1. Classic configuration

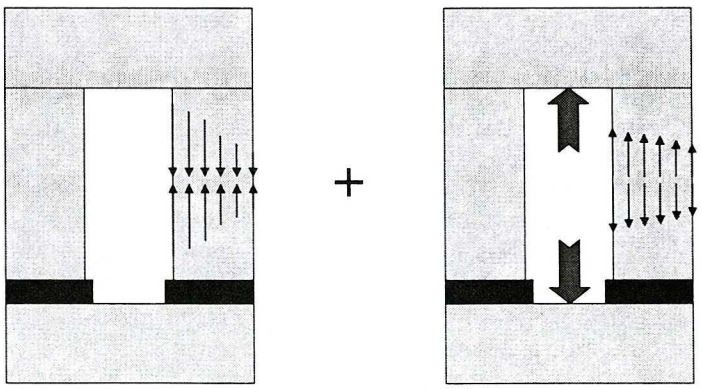

Fig. 2. Press with pre-compressed columns

In order to reduce the stress level, columns are sometimes assembled in a pre-compressed state. The entity of such pre-compression is established, so that nominal stress remains negative throughout the cyclic loading phase. Nevertheless, it has been observed that even in pre-compressed columns, cracks can initiate and grow at a considerable rate. The present study investigates the causes of crack initiation and propagation in an industrial

press column. This press is able to generate a high vertical load (up to 46 MN) so that stiff components can be compressed. The compressive stress has been estimated by theoretical and experimental analyses, Fig. 2.

The opportunity to carry out a complete test campaign on a prototype has made it possible to verify assumptions and to evaluate several hypotheses in order to clarify the unusual behaviour of propagation under compressive state.

Pre-tightening loads are obtained through thin steel belts wrapped around the entire press shape for several turns. It was possible to estimate that $F_{V\,max.}$, the compressive load generated during assembly in the two columns' is about 20% higher than the maximum value of the vertical load during the loading phase. Through the evaluation of the columns and belts' stiffnesses, the forcing diagram is traced and shown in Fig. 3. The columns stiffness is much higher than the steel belts one, due to the large size of the two columns compared to the section of belts. The slopes of the two lines are very different, and the dotted line on the right can be well approximated to a horizontal one.

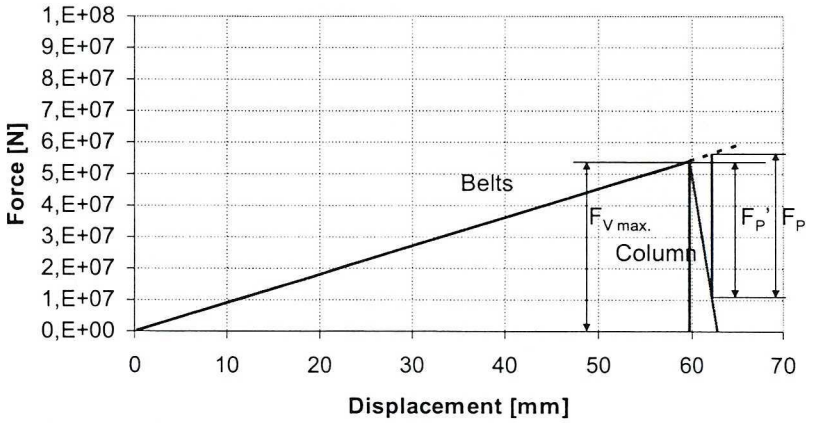

Fig. 3. Forcing diagram

F_P is the maximum value of work load transmitted by the piston and it is important to observe that in this condition the compressive load acting on the columns is reduced by a quantity $F_P' < F_P$. Because of the low slope of the "Belts" line, as suggested by the figure above, it is acceptable to suppose that $F_P \cong F_P'$, i.e. during the loading phase the extent of pre-compression is lowered by a quantity that is equal to the work load itself. Consequently the residual negative force acting on the columns can be calculated as $(F_{V\,max.} - F_P)$ instead of $(F_{V\,max.} - F_P')$.

The initiation of a crack could be noticed after half million work cycles. This crack, Fig. 4b, was located in one of the two low strength steel (Fe 510) columns, in the heat affected zone of a welded flange. The crack strongly increased in two directions of the sharp corner of the column, and after about 3.5 million cycles, it was about 200 mm long and 45 mm deep.

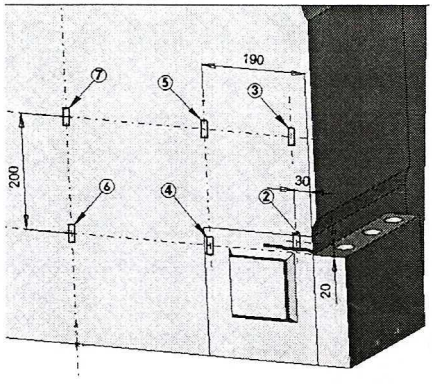

Fig. 4a. Strain gages arrangement

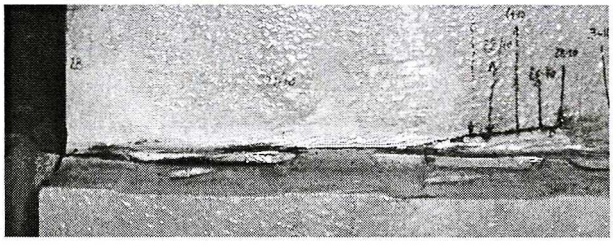

Fig. 4b. A photo of the crack

2. Measurement of stress variation by strain gage analysis

Several strain gages were located near the crack, in order to estimate loads acting on the column during the work cycle. The first tests estimate the values of strain during the loading phase. The data from strain gages 3, 5, 6 and 7, Fig. 4a, are the most reliable, since these gages are quite close to the cracked area, and sufficiently far not to be influenced by the crack presence. Strain variations were registered in the loading phase. Readings and medium values are shown in tab. 1: on the basis of such data, by applying the Hooke equation, the stresses were estimated.

Table 1.

Strain gages readings and elaborations

Strain gauge number	Medium readings [με]	Standard deviation [με]	Stress variation [MPa]
3	376	1.15	77
5	504	1.00	104
6	421	2.65	87
7	446	0.58	92

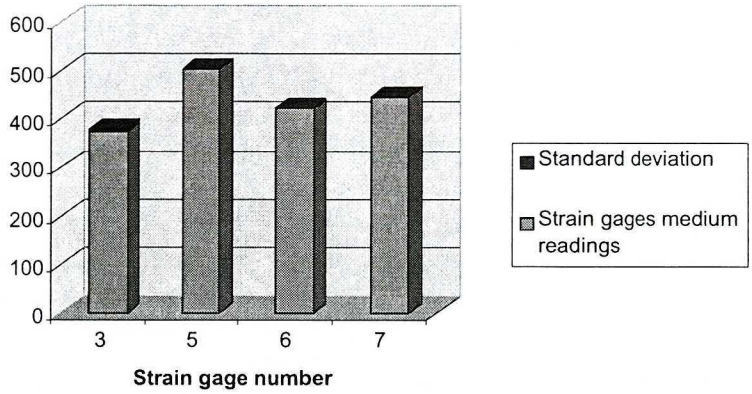

3. Estimation of pre-compression stress

The aim of other tests was to measure the intensity of pre-compression S_C in a no-work condition. Material all around strain gages was removed by mechanical cutting. In this way compressive loads were released, as confirmed by positive readings for strains. A medium value of $+580$ με has been obtained, corresponding to a stress of about -120 MPa. It can be concluded that the total stress remains negative throughout the work cycle.

4. Hysteresis loop in the welded structures and crack nucleation

A welding in a corner, connecting a flange on the front size of a column, was considered as the possible first cause of crack initiation.

Due to the welding process and to differential temperatures, the presence of a residual tensile stress can be hypothesized. Because of the difficulty of precise measurement, the residual stress in the welding was simply estimated as equal to the yield stress for this type of steel ($300 \div 315$ MPa). By using the local strain approach and the relative equations (1, 2, 3), the hysteresis loop in the welded area was estimated, Fig. 5b [1].

1. Following the technological and assembly processes and the loading cycle sequence, equation (1) describes the first path of the stress state, from zero to the maximum residual stress value. The yield value was estimated as equal to 300 ÷ 315 MPa, in accordance with [5]. Consequently, point A is located at the intersection between the curve (1) and the horizontal straight line $\sigma = \sigma_y$.
2. The columns are then pre-compressed during the assembly phase, and through the solution of the set of equations (2) it is possible to calculate stress and strain at point B.
3. Finally, the set of equations (3) describes stress and strain at point C that corresponds to the maximum work load and in this way the closed work cycle is described by the hysteresis diagram between point B and point C. Point C does not coincide with point A, because the maximum load is 20% lower than the pre-stressed one.

Fig. 5a shows the qualitative behaviour of the isostatic curves of the stress distribution due to the pre-compression of the columns. S_C is the nominal stress constant on the mean section. A value of 4.2 was estimated for the stress concentration factor with reference to nominal stress S_C. The estimation of the maximum stress in the corner D (indicated in Fig. 5a) was performed by finite element analysis, and the K_t factor was obtained by referring the maximum value to the nominal stress S_C (Fig. 5c).

$$\varepsilon_A = \frac{\sigma_A}{E} + \left(\frac{\sigma_A}{K}\right)^{1/n} \tag{1}$$

$$\begin{cases} \dfrac{(\varepsilon_A - \varepsilon_B)}{2} = \dfrac{(\sigma_A - \sigma_B)}{2E} + \left[\dfrac{(\sigma_A - \sigma_B}{2K'}\right]^{1/n'} \\ (\sigma_A - \sigma_B) \cdot (\varepsilon_A - \varepsilon_B) = \dfrac{[K_t \cdot (S_A - S_B)]^2}{E} \end{cases} \tag{2}$$

$$\begin{cases} \dfrac{(\varepsilon_C - \varepsilon_B)}{2} = \dfrac{(\sigma_C - \sigma_B)}{2E} + \left[\dfrac{(\sigma_C - \sigma_B}{2K'}\right]^{1/n'} \\ (\sigma_C - \sigma_B) \cdot (\varepsilon_C - \varepsilon_B) = \dfrac{[K_t \cdot (S_C - S_B)]^2}{E} \end{cases} \tag{3}$$

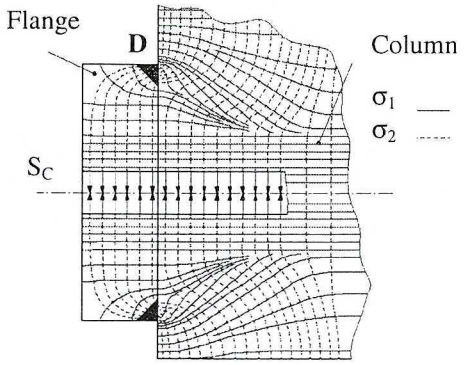

Fig. 5a. Qualitative stress distribution due to pre-compression of the columns

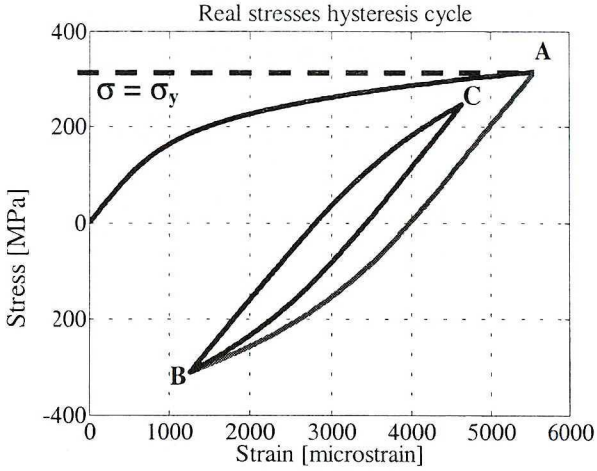

Fig. 5b. Stress – strain hysteresis diagram

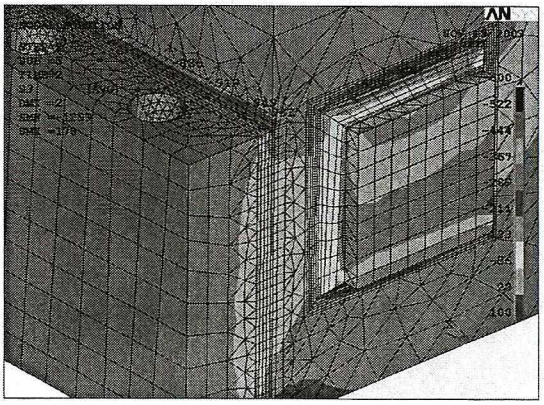

Fig. 5c. FEM analysis on stress maximum value in the corner D

$$\frac{\Delta\varepsilon}{2} = \frac{\sigma'_f - \sigma_m}{E} \cdot (2N)^b + \varepsilon'_f \cdot (2N)^c \tag{4}$$

By using the Manson Coffin model (4), it was possible to estimate the number of working cycles up to crack nucleation. This number, $4.5 \cdot 10^5$ cycles, appears to be highly consistent with the number observed during machine work, in fact the first visible crack was detected after about half million cycles.

5. The reversed flow plastic zone effect

By looking at the diagram above, it can be noted that the minimum stress value (state B) is beyond yield compression threshold $-\sigma_y$. It is reasonable to suppose that, after initiation, the crack is surrounded by a compression yielded zone. Literature research has shown that a compressive overload can be the cause of crack propagation even if the stress intensity factor related to the following load is below the threshold [6], [7], [9], [10], [11]. In [8] a first explanation is given: in a cracked specimen subjected to compressive cyclic load, a residual tensile stress is generated at the crack tip when the maximum load is released.

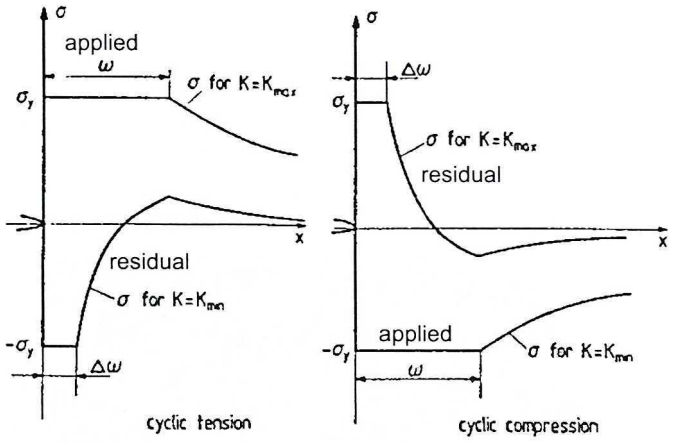

Fig. 6. Applied and residual stress (cyclic tension and cyclic compression) [9]

In [9] it is specified (see Fig. 6 on the right) that when the maximum compressive load is released, the yield in tension is reached. The same theory can be used also in the case of a positive cyclic stress (see Fig. 6 on the left): if a positive yield is reached at maximum load, stress decreases to the negative yield stress after the load release. This is a very well known effect and is used

in order to prevent crack propagation in large pressure vessels. This effect, the "reversed flow plastic zone effect" is explained in [1], with reference to a cracked specimen subjected to cyclic nominal compressive load, Fig. 7.

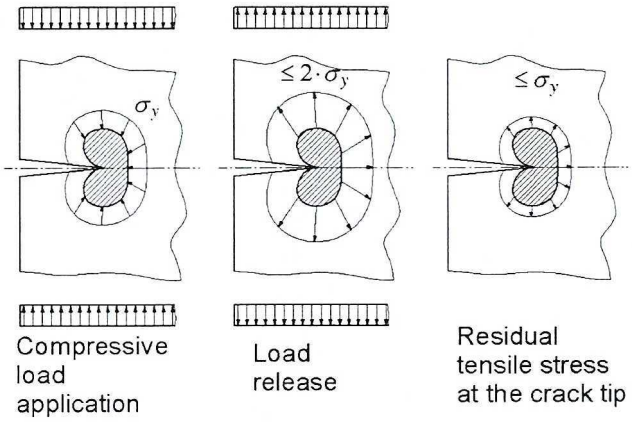

Fig. 7. Graphic representation of the reversed flow plastic zone effect

When maximum compressive load is applied (on the left), a compression yielded zone is generated at the crack tip, then at load release (i.e. during component compression, point C in the hysteresis cycle), the material tends to relax, but such relaxation is prevented by permanent deformation. As a consequence, a residual tensile stress is generated, as is shown in the final configuration on the right.

6. Primary crack propagation

The graphic in Fig. 8 from [8] shows that, as the number of cycles increases, the crack length increases to reach an asymptotic value, which means the crack propagation rate decreases to zero. The reversed flow plastic zone effect is able to explain only the primary propagation, but not the secondary one that has been observed in the present case. Direct monitoring on the press columns shows that, in spite of the information contained in diagram below, the crack is still propagating, with a considerable rate.

A possible explanation of the secondary propagation is provided by the following observation.

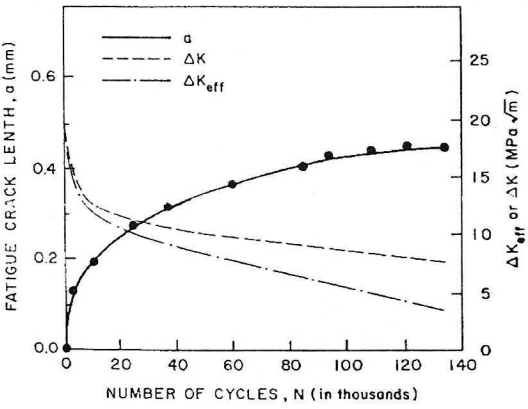

Fig. 8. Relationship between the crack length and the number of cycles [8]

7. Secondary crack propagation

The primary crack propagation and related final arrest of the crack does not properly represent the actual phenomenon. A clear experimental evidence demonstrates that a secondary propagation takes place, since the distribution of strain along the crack axis has an approximately hyperbolic shape as shown in Fig. 9 (experimental curve).

Strain variations at the crack tip (angular direction for $\theta = 0$) during the working cycle were estimated by strain gage measurements, Fig. 9 and Tab. 2. A chain of nine active gage grids was used for this test. As the Wheatstone bridges are balanced before load application, the readings do not take into account the effect of pre-compression on columns. Since the experimental curve is related only to work load cycle, it does not represent the real strain distribution nearby the crack tip. With reference to a crack closure model, it seems to be empirically correct to lower the measured strain by a quantity that is equal to pre-compression strain estimated in par. 1 and 3 (equal to 580 $\mu\varepsilon$, according also to the forcing diagram profile previously reported). The points in the low part of fig. 9 represent the real strain curve. Consequently, a large zone at the crack tip becomes in tension in the phase of load application. Finally, experimental evidence makes sure that propagation according to mode I is present. Moreover during the loading phase the crack opening displacement becomes quite evident, which confirms the presence of a tensile state of stress. The explanation of the phenomenon is the following. Crack itself generates a redistribution of the stress state: because of not negligible crack extension, the column starts to be subjected to a bending moment effect, which justifies the generation of a tensile stress.

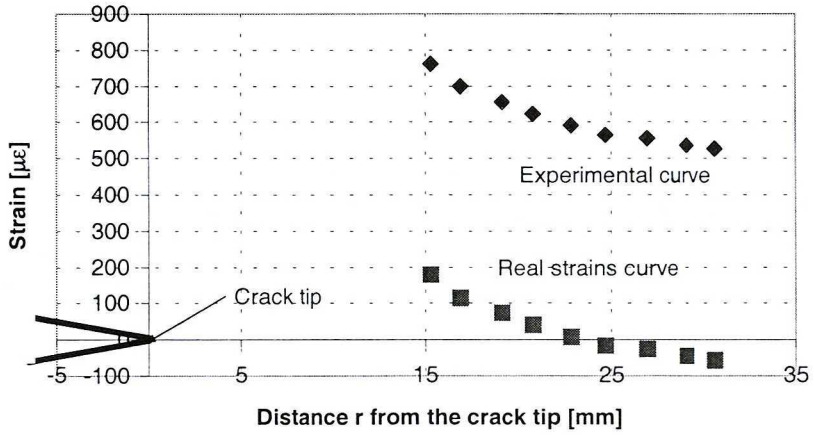

Fig. 9. Experimental results of strain gage measurements

Table 2.

Stress intensity factor estimation

Distance from the crack tip r [mm]	Measured strains [με]	Real strains [με]	$\sqrt{2\pi r}$ $\left[\sqrt{mm}\right]$	K_I $\left[MPa\sqrt{mm}\right]$
15.3	762	179	9.80	419
16.9	699	116	10.30	279
19.15	656	73	10.97	184
20.8	623	40	11.43	104
22.8	591	8	11.97	22
24.7	566	−17	12.46	–
26.9	557	−26	13.00	–
29.1	537	−46	13.52	–
30.7	527	−56	13.89	–

In the following step, experimental data allow an estimation of the stress intensity factor and of the crack propagation rate. According to the three-term model for the stress field around the crack tip and to the Hooke law, it is possible to write equations (5) and (6). Let σ and ε be stress and strain along both horizontal and vertical Cartesian coordinates at angular direction for $\theta = 0$

$$\sigma = \frac{K_I}{\sqrt{2\pi r}} + \frac{3}{4}\frac{K_I}{\sqrt{2\pi r}}\frac{r}{a} - \frac{5}{32}\frac{K_I}{\sqrt{2\pi r}}\left(\frac{r}{a}\right)^2 \tag{5}$$

$$\varepsilon = \frac{1 - \nu}{E}\sigma \tag{6}$$

Combining (5) and (6) in equation (7) makes it possible to calculate a value of the stress intensity factor K_I for each of the experimental data corresponding to different distances from the crack tip:

$$K_I = \frac{\dfrac{E\,\varepsilon}{1 - \nu}}{\dfrac{1}{\sqrt{2\pi r}} + \dfrac{3}{4}\cdot\dfrac{1}{\sqrt{2\pi r}}\cdot\dfrac{r}{a} - \dfrac{5}{32}\cdot\dfrac{1}{\sqrt{2\pi r}}\cdot\left(\dfrac{r}{a}\right)^2} \tag{7}$$

Different values of the stress intensity factor are estimated at different distances r from the crack tip. It is possible to note that the stress intensity factor decreases as the distance becomes higher with linear distribution (as plotted in Fig. 12). The equation of the best fit interpolating line (8) is:

$$K_I = -135.6\cdot\sqrt{2\pi}\cdot\sqrt{r} + 1684.6 \tag{8}$$

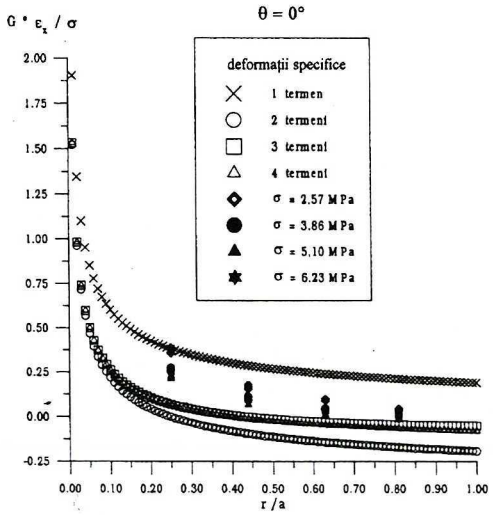

Fig. 10a. Relationship between theoretical and experimental results [3]

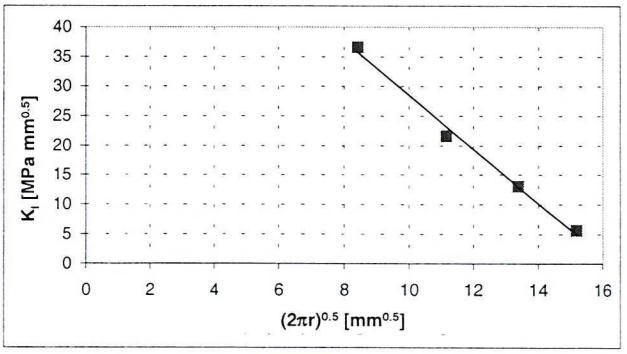

Fig. 10b. Stress intensity factor distribution as an elaboration of Constantinescu's experimental results

In the theoretical case, this line should be horizontal, i.e. the stress intensity factor should not vary with the distance. However, recent experiences by Constantinescu, Fig. 10a [3] have shown that strain values decrease with respect to distance with a slope higher than the theoretical one. These results were obtained for (r/a) ranging from 0.25 to 0.8: for a crack depth a equal to 45 this range corresponds to a distance from 11 to 36 mm. Since strain gage chain grids were located at distances from 15 mm to 31 mm, this ensures that the present results can be compared to [3]. The diagram in Fig. 10b is an elaboration of the results shown on the left: by the application of equation (7), the stress intensity factor is expressed with dependence on the square root of the distance. Also in this case, a linear distribution with negative slope is obtained.

The following step of the study was to evaluate an acceptable value for the stress intensity factor. The presented stress model is a singular one, since stress tends to infinity when the distance from the crack tip tends to zero. In reality, stress cannot exceed the yield value because of stress redistribution.

It can be observed that the stress intensity factor is correctly defined at a sufficiently low distance from the crack tip. For this reason it appeared acceptable to estimate the value of K_I at the border of the plastic zone [4]. Fig. 11 indicates that the direct estimation of K_I, neglecting the redistribution of stress due to the plastic zone size, is not fully correct. A more reliable value of K_I can be estimated at the border of the plastic zone (i.e. at a distance $r_{pl.}$ from the crack tip, or, that is the same, at the fictitious crack tip, indicated with dashed line in Fig. 11). Since the plastic zone size depends on the K_I value, the K_I estimation at the border of the plastic zone can be carried out only by an iterative method. The equations (8) and (9) were applied, the last one is the relationship between the stress intensity factor and the plastic radius.

$$\sigma_x = \sigma_y = \sigma = \frac{K_I}{\sqrt{2\pi r_{pl.}}} + \frac{3}{4}\frac{K_I}{\sqrt{2\pi r_{pl.}}} \cdot \frac{r_{pl.}}{a} - \frac{5}{32}\frac{K_I}{\sqrt{2\pi r_{pl.}}} \cdot \left(\frac{r_{pl.}}{a}\right)^2 = \sigma_y \Rightarrow r_{pl.} \tag{9}$$

The iterative process starts with the choice of a possible value of the stress intensity factor. Then, at the generic (i-th) step, a value of K_I ($K_{I_{(i)}}$) is known from the previous one. By employing (9) it is possible to calculate the current value of the plastic radius and to determine its square root and finally, by using the interpolating equation (8), a new value for K_I, $K_{I_{(i+1)}}$. This result constitutes the input for the following iteration step. The procedure is synthesized by formulas (10, 11) and by the diagram in Fig. 12.

$$K_{I_{(i)}} = 896 MPa\sqrt{mm} \tag{10}$$

$$\sigma_x = \sigma_y = \sigma = \frac{K_{I_{(i)}}}{\sqrt{2\pi r_{pl.\,(i+1)}}} + \frac{3}{4}\frac{K_{I_{(i)}}}{\sqrt{2\pi r_{pl.\,(i+1)}}} \cdot \frac{r_{pl.\,(i)}}{a} - \frac{5}{32}\frac{K_{I_{(i)}}}{\sqrt{2\pi r_{pl.\,(i+1)}}} \cdot \left(\frac{r_{pl.\,(i+1)}}{a}\right)^2 =$$

$$= \sigma_y \Leftrightarrow \frac{896}{\sqrt{2\pi r_{pl.\,(i+1)}}} + \frac{3}{4}\frac{896}{\sqrt{2\pi r_{pl.\,(i+1)}}} \cdot \frac{r_{pl.\,(i+1)}}{45} - \frac{5}{32}\frac{896}{\sqrt{2\pi r_{pl.\,(i+1)}}} \cdot \left(\frac{r_{pl.\,(i+1)}}{45}\right)^2 =$$

$$= 315 \Leftrightarrow \sqrt{r_{pl.\,(i+1)}} = 1.16\sqrt{mm} \Leftrightarrow r_{pl.\,(i+1)} = 1.34 mm \tag{11}$$

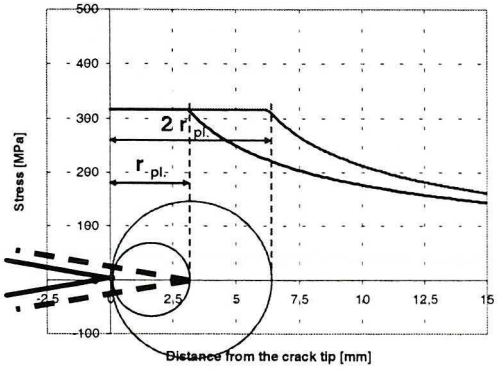

Fig. 11. Stress redistribution at the crack tip

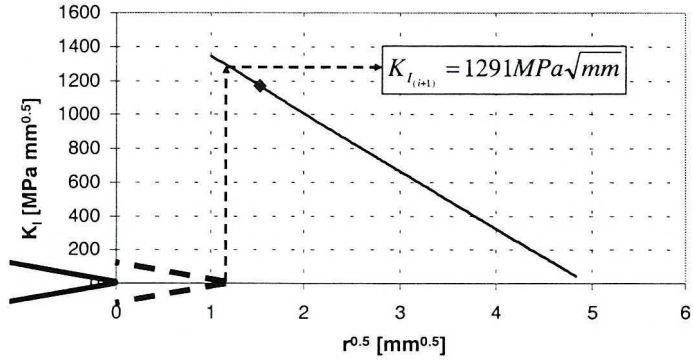

Fig. 12. Iterative process for the stress intensity factor determination

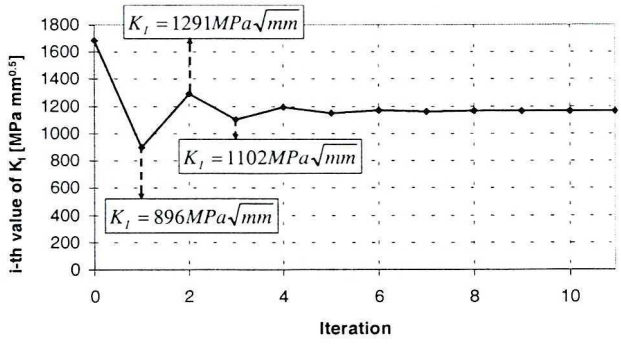

Fig. 13. Convergence of the iterative process for stress intensity factor calculation

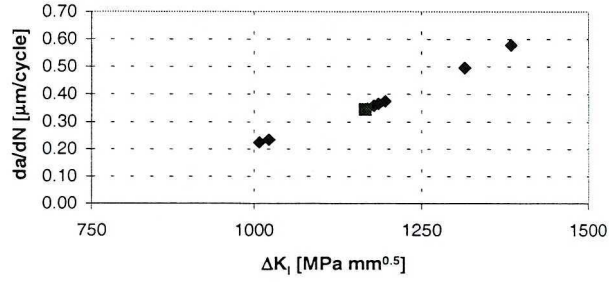

Fig. 14. Estimation of the crack propagation rate and comparison to monitored one

After about 10 iterations, Fig. 13, values of 1165 $MPa\sqrt{mm}$ for the stress intensity factor and of 2.3 mm for the plastic radius $r_{pl.}$ were estimated (marker in Fig. 12). In order to obtain confirmation for the calculated K_I, the crack propagation rate was estimated by using the Paris law (12) and was compared to direct monitoring on the machine.

$$\frac{da}{dN} = C \cdot \Delta K^m \cong 0.35 \mu m/cycle \tag{12}$$

This value (red marker), though estimated by an approximated law, is close to the mean one observed for the crack propagation rate (Fig. 14).

8. Second order effects

Experimental measurements made it possible to estimate shear displacements between points A – B and C – D. The maximum extent of such displacements was about 40 μm. Then, a possible influence of K_{II} and K_{III} can be hypothesized.

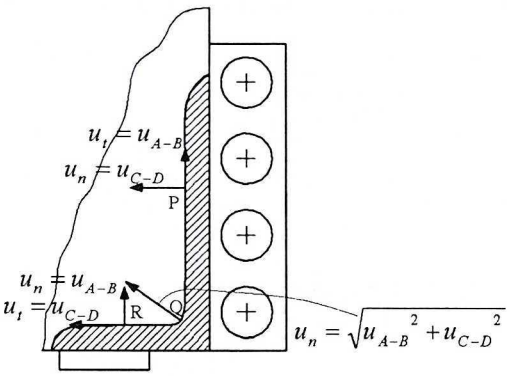

Fig. 15a. Meaning of displacement terms

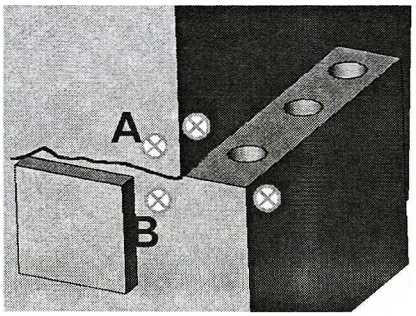

Fig. 15b. Collocations of points A, B, C, D

$$K_{II} = \frac{u_n G\sqrt{\pi}}{\sqrt{2r}\cdot(1-\nu)} = \frac{u_n E\sqrt{\pi}}{\sqrt{2r}\cdot 2\cdot(1-\nu)(1+\nu)} \tag{13}$$

$$K_{III} = \frac{u_t G\sqrt{\pi}}{\sqrt{2r}} = \frac{u_t E\sqrt{\pi}}{\sqrt{2r}\cdot 2\cdot(1+\nu)} \tag{14}$$

The obtained values are quite relevant, in particular 1163 $MPa\sqrt{mm}$ for K_{II} and 660 $MPa\sqrt{mm}$ for K_{III}, consequently also propagation according to modes II and III cannot be excluded.

9. Conclusions

On the basis of the evidence of the experiments, the fracture phenomenon in compression can be explained and modelled as follows:

- the corner and the welded joint are responsible for the nucleation, because of residual tensile stress;
- the "reversed flow plastic zone effect" can explain a primary propagation;
- at the larger extension of the crack, stress intensification at the crack tip related to a bending moment effect (during the loading phase) prevails on the nominal compression and is able to justify a secondary propagation.
- This "reversed flow plastic zone effect" is generated not only at the crack tip, but also in all the points where the yield compression strength is overcome. Consequently, a good design solution is to avoid any corners and discontinuities that could locally amplify the pre-compression nominal stress, which may lead to overcome the yield threshold: these points during the loading phase become stressed in tension.
- It is not possible to exclude a synergic effect on the propagation due to modes II and III. However this effect is only a second order one, being the first mode, clearly visible, the prevailing one.

Manuscript received by Editorial Board, February 07, 2005;
final version, September 23, 2005.

REFERENCES

[1] Ralph I. Stephens, Ali Fatemi, Robert R. Stephens, Henry O. Fuchs: Metal Fatigue in Engineering, John Wiley & Sons Inc., New York, 2001.
[2] Rolfe, Barsom: Fracture and fatigue control in structures – Applications of fracture Mechanics, Prentice-Hall Inc., Englewood Cliffs, New Jersey, 1977.
[3] Dan Mihai Constantinescu: Dezvoltari si aplicatii in mecanica ruperii si oboseala, Editura Academiei Romane, Bucurest, 2003.
[4] Ewalds E. L., Wanhill R. J. H.: Fracture Mechanics, Edward Arnold Ltd, London, 1984.
[5] Niemann, Winter: Maschinen – Elemente, Band. 1, Sprinter-Verlag Berlin, Heidelberg , 1981.
[6] Reid C.N., Williams K., Hermann R.: Fatigue in compression. Fatigue Engineering Materials Structures, Vol. 1, 1979, pp. 267÷270.
[7] Zaiken E., Ritchie R. O.: On the role of compression overloads in influencing crack closure and the threshold condition for fatigue crack growth in 7150 aluminium alloy. Engineering Fracture Mechanics, Vol. 22, 1985, pp. 35÷48.

[8] Suresh S.: Crack initiation in cyclic compression and its applications. Engineering Fracture Mechanics, Vol. 21, 1985, pp. 453÷463.
[9] Pippan R.: The growth of short cracks under cyclic compression. Fatigue Fracture Engineering Materials Structures, Vol. 9, 1987, pp. 319÷328.
[10] Grasley A.: Influence of residual welding stresses, overload and specimen preparation on fatigue crack growth under axial compression. Engineering Fracture Mechanics, Vol. 50, 1995, pp. 407÷415.
[11] Vasudevan A. K., Sadananda K.: Analysis of fatigue crack growth under compression – compression loading. International Journal of Fatigue, Vol. 23, 2001, pp. 365÷374.

Powstawanie i rozwój pęknięć w kolumnach prasy pod wpływem obciążenia ściskającego

Streszczenie

Jedna z najgroźniejszych awarii, jaka może wystąpić w prasach przemysłowych, jest związana z ryzykiem powstawania pęknięć w kolumnach. By uniknąć narażenia kolumn prasy na naprężenia rozciągające w fazie obciążenia, przy montażu kolumn wprowadza się niekiedy kompresję wstępną, dzięki czemu nominalne naprężenia zachowują wartości ujemne przez cały cykl roboczy.

Poprzednie badania dotyczyły rozwoju pęknięć powstających w próbkach z nacięciem pod wpływem obciążenia okresowo zmiennego. W tych przypadkach pęknięcia zmęczeniowe są inicjowane u podstawy nacięcia jako wynik resztkowego naprężenia rozciągającego i rozwijają się z prędkością malejącą stopniowo aż do zatrzymania. Przedmiotem obecnej pracy jest pokazanie paradygmatycznego przykładu powstawania i rozwoju pęknięć także w ogólnym polu naprężeń ściskających.